ACS Biomaterials SCIENCE & ENGINEERING

pubs.acs.org/journal/abseba

Article

# Collagen I Based Enzymatically Degradable Membranes for Organ-on-a-Chip Barrier Models

Yusuf B. Arık,[†] Aisen de sa Vivas,[†] Daphne Laarveld, Neri van Laar, Jesse Gemser, Thomas Visscher, Albert van den Berg, Robert Passier, and Andries D. van der Meer*

Cite This: *ACS Biomater. Sci. Eng.* 2021, 7, 2998–3005

Read Online

ACCESS | Metrics & More | Article Recommendations | Supporting Information

**ABSTRACT:** Organs-on-chips are microphysiological in vitro models of human organs and tissues that rely on culturing cells in a well-controlled microenvironment that has been engineered to include key physical and biochemical parameters. Some systems contain a single perfused microfluidic channel or a patterned hydrogel, whereas more complex devices typically employ two or more microchannels that are separated by a porous membrane, simulating the tissue interface found in many organ subunits. The membranes are typically made of synthetic and biologically inert materials that are then coated with extracellular matrix (ECM) molecules to enhance cell attachment. However, the majority of the material remains foreign and fails to recapitulate the native microenvironment of the barrier tissue. Here, we study microfluidic devices that integrate a vitrified membrane made of collagen-I hydrogel (VC). The biocompatibility of this membrane was confirmed by growing a healthy population of stem cell derived endothelial cells (iPSC-EC) and immortalized retinal pigment epithelium (ARPE-19) on it and assessing morphology by fluorescence microscopy. Moreover, VC membranes were subjected to biochemical degradation using collagenase II. The effects of this biochemical degradation were characterized by the permeability changes to fluorescein. Topographical changes on the VC membrane after enzymatic degradation were also analyzed using scanning electron microscopy. Altogether, we present a dynamically bioresponsive membrane integrated in an organ-on-chip device with which disease-related ECM remodeling can be studied.

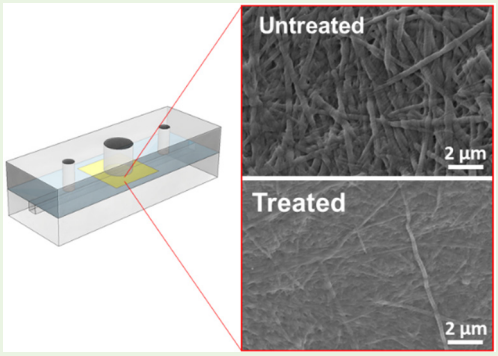


**KEYWORDS:** *vitrified collagen membrane, organ-on-a-chip, permeability, collagenase*

## INTRODUCTION

The extracellular matrix (ECM) is the noncellular component of tissues and organs. Not only does it provide physical support to cells, it initiates biochemical and biomechanical cues.[1] ECM is composed of a great variety of molecules such as collagen-family proteins, glycosaminoglycans, proteoglycans, and adhesive glycoproteins. Different organization of these components gives rise to different tissue characteristics. Collagens, in particular type I, II, and III, are the most abundant proteins in the human body.[2] Collagens are responsible for key tissue-level functions such as cell attachment and spreading, in addition to mechanical and structural functions. Furthermore, these properties have an influence on cellular differentiation and movement.[3] The importance of ECM is also illustrated by the wide variety of diseases that arise from genetic abnormalities in ECM proteins.[4]

Considering the significance of the ECM in fundamental cellular processes and disease pathologies,[4] experimental models where changes to tissues can easily be observed and experimental conditions can be manipulated are needed. In recent years, microfluidic organ-on-a-chip devices have been proven to be promising in in vitro disease modeling platforms that recapitulate human specific physiology.[5−12] These devices are miniaturized cell culture platforms comprising defined microchannels that are inhabited by living cells to mimic tissue−organ level physiology. Depending on the research question, physicochemical parameters of the native tissue environment can be incorporated. Whereas simple devices contain only one type of cell cultured in a perfusable chamber, more complex devices have multiple channels separated by semipermeable porous membranes lined by two or more type of cells.

These semipermeable membranes located between adjacent culturing chambers in organs-on-chips aim to mimic the basement membrane, a type of ECM creating boundaries between tissues. Moreover, these membranes provide physical anchoring points for cells while enabling compartmentalization. This is due to its porous structure, which prevents cell

**Special Issue:** Beyond PDMS and Membranes: New Materials for Organ-on-a-Chip Devices

**Received:** May 26, 2020
**Accepted:** February 18, 2021
**Published:** February 24, 2021

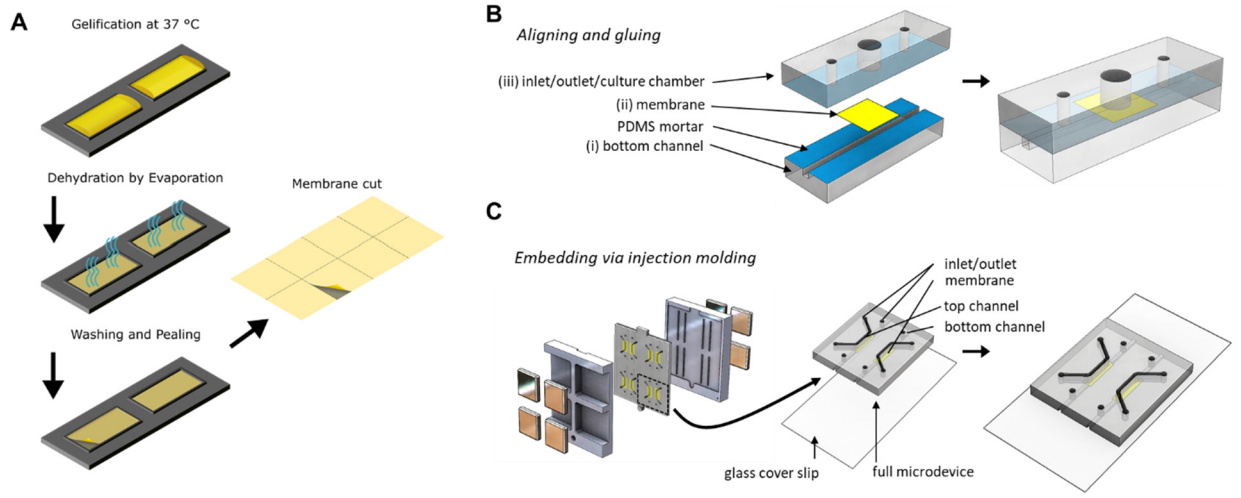


**Figure 1.** Fabrication of vitrified collagen membrane and organ-on-a-chip device in which the membranes were integrated. (A) Vitrified collagen membranes were fabricated by depositing a neutralized collagen solution on a PDMS slab with defined rectangular shapes, which was subsequently dried in aseptic conditions. This resulted in a thin film of collagen along with salts and other phenol red. Following drying, the collagen film was washed with deionized water to remove salts and phenol red. After a second drying process, a thin film of collagen was obtained, which was easily handled and could be incorporated into the organ-on-a-chip device. (B) PDMS-based organ-on-a-chip device with exploded view (left) and assembled final device (right). The device contains a 1 $mm^2$ square microchannel (i), at the center of which the membrane (ii) was located. There is an open-top culture chamber (3 mm Ø) situated above the membrane (iii). PDMS layers were assembled by applying mortar to surfaces (blue, I and III) to sandwich the membrane in between. (C) Injection molding was used to eliminate the labor intensive fabrication procedure. (Left) Different layers of the device were assembled by incorporating the collagen I based membranes in between the channels held by magnets on each end. (Middle) Final assembled device consists of a PDMS-coated glass coverslip, a square microchannel, collagen-based membrane stretched in the center, and another square microchannel on top. (Right) The final assembled layer requires only plasma activation of surfaces to be attached to glass coverslip.

migration and allows exchange of soluble signaling cues through the pores. Despite being widely used in organs-on-chips, porous membranes are usually made of synthetic polymers (e.g., poly dimethylsiloxane (PDMS), polycarbonate, polyester) which differ from ECM found in vivo. They are often coated with ECM proteins (e.g., fibronectin, collagen, laminin, or Matrigel) to enhance attachment of anchorage-dependent cells to the membrane surface, rendering the membranes more bioactive.[13,14] Despite these efforts, the majority of the material remains synthetic and fails at mimicking biochemical cues that affect the structure and function of cells as well as the fibrillar ultrastructure of basement membranes.[15] Furthermore, custom fabrication of synthetic membranes from alternative materials or with engineered properties requires dedicated systems such as track etching,[16] chemical etching,[17] phase inversion,[18] and electrospinning.[19]

Previous studies used either ex vivo basement membranes or vitrified membranes fabricated using different configurations of natural hydrogels to address these challenges.[20−29] For example, Mondrinos et al.[21] reported membranes that use three-step fabrication (gelation, dehydration, and vitrification). The resulting membranes are thin, fibrillar, and stable enough to be incorporated into a microfluidic device. Although these studies demonstrate the feasibility of integrating these membranes in microfluidic chips, none of them provide full characterization of the incorporated membranes in terms of ultrastructure, enzymatic degradation, and dynamic permeability or simplification of the integration process in organs-on-chips.

Here, we report a collagen I based membrane incorporated in an organ-on-chip device. In our study, we study membrane ultrastructure and permeability, as well as adhesion of both endothelial and epithelial cells. Moreover, we characterize the degradation and remodeling of the basement membrane by a protease. In addition, we provide an injection molding design to fabricate our devices, which eliminates the labor intensive utilization of the toxic PDMS mortar to incorporate the membranes between channels. Our study reinforces the notion that vitrified collagen membranes have strong added value in organ-on-chip engineering.

## EXPERIMENTAL SECTION

**Membrane Fabrication.** Collagen I based membranes were prepared via multistep procedure depicted in Figure 1A. First, rat tail collagen type I (VWR, The Netherlands) was prepared according to the manufacturer's instructions at a concentration of 3 mg/mL and a pH between 7.5 and 8 by mixing with $dH_2O$, phosphate buffered saline (PBS, ThermoFisher, USA), and 1 M sodium hydroxide solution. Afterward, the collagen solution was pipetted evenly onto a PDMS slab (0.25 mL/$cm^2$). This was followed by overnight dehydration in aseptic conditions at room temperature (RT). Evaporation of water resulted in a thin film of collagen on the surface of PDMS. Subsequently, this collagen film was rehydrated with $dH_2O$ for 4 h at RT to remove salts and other impurities. Membranes underwent another drying cycle after gentle aspiration of water. Following this second dehydration step, membranes were cut into chip sized pieces (~6 $mm^2$).

Following incorporation to devices, membranes were enzymatically treated. First, collagenase II was diluted in PBS to a desired concentration (24, 48, 120 U/mL) and pipetted onto membranes. Afterward, devices were incubated for 5 min at 37 °C with 5% $CO_2$.

Following treatment, collagenase II was removed from the culture chamber, and membranes were washed with PBS to remove any remaining enzyme.

To generate multilayered membranes, we prepared collagen membranes with 3 and 4 mg/mL collagen I as mentioned. A second layer of the membrane was placed onto the first layer following the addition of 10 mU/mL transglutaminase (Ajinomoto, Germany) in


https://dx.doi.org/10.1021/acsbiomaterials.0c00297
ACS Biomater. Sci. Eng. 2021, 7, 2998−3005

PBS onto the first dehydrated membrane for 2 h at 37 °C. Following incubation, the membranes were washed three times with PBS. Cross sections of membranes were done by first immersing the double-layered membranes in liquid nitrogen until they were completely frozen and then manually breaking the layers.

**Chip Fabrication.** Casted poly(methyl methacrylate) (PMMA, Altuglass) master molds containing channel imprints were first designed using Solidworks and fabricated with a computer numerical control (CNC) milling machine (Datron Neo, Datron AG). Afterward, PDMS base and curing agent were mixed at a ratio of 10:1 (wt: wt) (Sylgard 184 Silicone elastomer kit, Dow Corning). It was then degassed and poured onto the positive PMMA molds and subsequently cured for at least 3 h at 65 °C. After that, cured PDMS was separated from the molds as slabs. PDMS slabs with square microchannels (1 $mm^2$) were cut from each side to generate side inlets (Figure 1B-i). After that, 2 inlets and 1 culture chamber (1.2 mm and 3 mm in diameter respectively) were punched into the PDMS slab corresponding to the middle part of the final assembled device Furthermore, three reservoirs were punched (5 mm in diameter) into another PDMS slab for the top compartment of the assembled device (Figure 1B-iv). Subsequently, all three slabs were aligned and cut into device-sized pieces. Prior to assembly of the device parts, dust was removed by Scotch tape (3M). Leak-free assembly of the parts was achieved by using uncured PDMS/toluene mortar (5:3 wt ratio) (toluene from Merck) as previously reported.[30,31] First, this mixture was spin-coated onto a glass coverslip (1500 rpm, 60 s, 1000 rpm/s, Spin150, Polos) and transferred to the device parts with an ink roller. Second, membranes were cut into small squares (~36 $mm^2$) (Figure 1B-Membrane), aligned and sandwiched between the center of the bottom (Figure 1B-i) and middle (Figure 1B-iii) compartments. Afterward, assembled parts were baked overnight at 65 °C. Finally, the surfaces of the top compartment and the preassembled device were exposed to air plasma (50 W) for 40 s (Cute, Femto Science). After plasma treatment, activated surfaces were pressed together to complete the assembly of the device.

In addition to mortar-assembled devices, injection molding was used to incorporate membranes. First, collagen membranes were wetted to attach to top channel imprints in PMMA molds. This was followed by closing the bottom mold and applying four magnets per side from each end to hold the membrane in between during PDMS injection. Afterward, PDMS was freshly prepared and mixed as aforementioned with additional carbon powder (1 wt %:vol ratio, Vulcan XC-72R, Fuel Cell Store). The mixture was then injected through the inlet of the mold using a syringe (Norm-Ject, Henke Sass Wolf). As soon as the mold was filled with PDMS, syringe was removed and mold inlet was sealed with cured PDMS. The final mold was first incubated for 30 min at RT to eliminate any air bubbles, and was then baked for at least 3 h at 65 °C.

**Permeability Assay.** *On-Chip.* The permeability of vitrified collagen membranes was measured by means of fluorescein diffusion. First, the culture chamber (Figure 1B-iii) was filled with phosphate buffered saline (PBS, ThermoFisher). Second, 200 μg/mL fluorescein sodium salt (0.3 kDa, SigmaAldrich) diluted in PBS was pipetted into the microchannel (Figure 1B-i). After that, from the beginning of the experiment, a sample of 5 μL was collected from the culture chamber every 15 min and the levels were normalized by adding PBS to the culture chamber. To ensure homogeneity of the dye concentration along the microchannel, we transferred dye from one inlet to the other after every sampling. To avoid flow from the microchannel to the culture chamber, we maintained fluid levels in the culture chamber at the same level as the highest inlet (Figure S1A–C).

These samples were read by a plate reader (Victor3, PerkinElmer). Using a standard curve, fluorescence values were matched with concentrations. The permeability ($P_{membrane}$) of membranes was calculated by

$$P_{membrane} = \frac{dc}{dt}\frac{Volume_{chamber}}{C_i Area_{chamber}}$$

where $P_{membrane}$ is the permeability in cm/s, $C_i$ the initial fluorescein concentration in μg/mL, $Area_{chamber}$ and $Volume_{chamber}$ are the dimensions of the culture chamber in $cm^2$ and $cm^3$, and $dC/dt$ was the change in the concentration (μg/(mL s)).

Permeability measurements were repeated following enzymatic treatment of membranes.

*Transwell.* On-chip permeability assay with synthetic membranes were compared with conventional Transwell systems. The levels of solutions in both Transwell compartments were equalized to avoid pressure-driven fluid flow. Although the bottom well was filled with PBS, the inset was filled with 200 μg/mL fluorescein. Afterward, the permeability assay was carried out as described in the section above (Figure S1B, C).

**Imaging of Membranes.** Prior to imaging, membranes were fixed with fixation buffer that contains 2% paraformaldehyde (Sigma-Aldrich), 2.5% glutaraldehyde (Sigma-Aldrich) in 0.1 M sodium cacodylate buffer (sodium cacodylate trihydrate in ultrapure $H_2O$ at pH 7.4) overnight at 4 °C. Fixation buffer was gently aspirated and membranes were washed three times with cacodylate buffer. After that, membranes were treated with 2% osmium tetroxide solution in sodium cacodylate buffer for 1 h at RT. After osmium tetroxide treatment, membranes were washed again with sodium cacodylate buffer three times. Afterward, membranes were dehydrated progressively by submerging membranes in ethanol with increasing concentrations (70, 80, 90, and 100%) for 5 min at RT. This was followed by drying membranes with a critical drying point apparatus (Leica EM CPD030) according to manufacturer's instructions.

Following fixation, membranes were sputtered with gold (Sputter Coater 108auto, Cressington Scientific Instruments) for imaging with scanning electron microscope (SEM, JSM-IT100, JEOL).

**Cell Culture.** Human immortalized retinal pigment epithelial cells (ARPE-19, ATCC) were cultured with DMEM/F12 (with GlutaMAX, ThermoFisher) supplemented with 10% fetal bovine serum (FBS) and 50 U/mL penicillin/streptomycin (P/S). ARPE-19 cells were cultured in noncoated T75 flasks. Human iPSC derived endothelial cells (hiPSC-EC) were derived from a healthy control hiPSC line as described previously.[32] hiPSC-EC were cultured in human endothelial serum free medium (ThermoFisher) supplemented with 1% platelet poor plasma derived serum (BioQuote), 0.6 μg/mL VEGF (R&D Systems), and 0.2 μg/mL FGF (Milteny) in collagen coated flasks (0.1 mg/mL). The cells were incubated at 37 °C in humidified air with 5% $CO_2$. Flasks with confluent monolayers were either used for experiments or subcultured. ARPE-19 and hiPSC-EC were kept in culture up to passage number 30 and 4, respectively.

Prior to staining, ARPE-19 and hiPSC-EC cells were seeded on membranes. hiPSC-EC and ARPE-19 cells were obtained from a confluent flask using 1× Tryple (ThermoFisher) and 0.05% Trypsin-EDTA (ThermoFisher), respectively.

**Cell Staining.** Cells cultured on membranes were stained for cell specific adhesion markers, actin filaments and nuclei for confirmation of cell monolayers and their health. First, cells were washed with PBS and fixed with 4% formaldehyde (in PBS, ThermoFisher) for 15 min at RT. Following fixation, cells were washed 3 times with PBS. After that, cells were permeabilized for 60 min at RT with permeabilization buffer (PB), which contains 0.1% Triton X-100 (Sigma-Aldrich) and 10 mg/mL bovine serum albumin (BSA) in PBS. Afterward, ARPE-19 were incubated with mouse antihuman ZO-1 IgG (5 μg/mL in PB, BD Transduction Laboratories) for 2 h at RT. Following incubation, the cells were rinsed three times with PBS and washed three times with PBS for 10 min at RT. After that, the cells were incubated with 1.25 μg/mL 4′,6-diamino-2-Phenylindole (DAPI, ThermoFisher), 2 drops/mL ActinGreen (binds to actin filaments, ThermoFisher), donkey antimouse IgG Alexa Fluor 647 (5 μg/mL, ThermoFisher) in PB for 1 h at RT.

The cells were imaged with phase contrast, fluorescence microscopy using the EVOS FL Cell Imaging System (Life Technologies; GFP filter (ex 470/22 em 510/42) for ActinGreen, Cy5 filter (ex 628/40 em 692/40) for ZO-1 and DAPI filter (ex 357/44 em 447/60) for DAPI).


https://dx.doi.org/10.1021/acsbiomaterials.0c00297
ACS Biomater. Sci. Eng. 2021, 7, 2998−3005

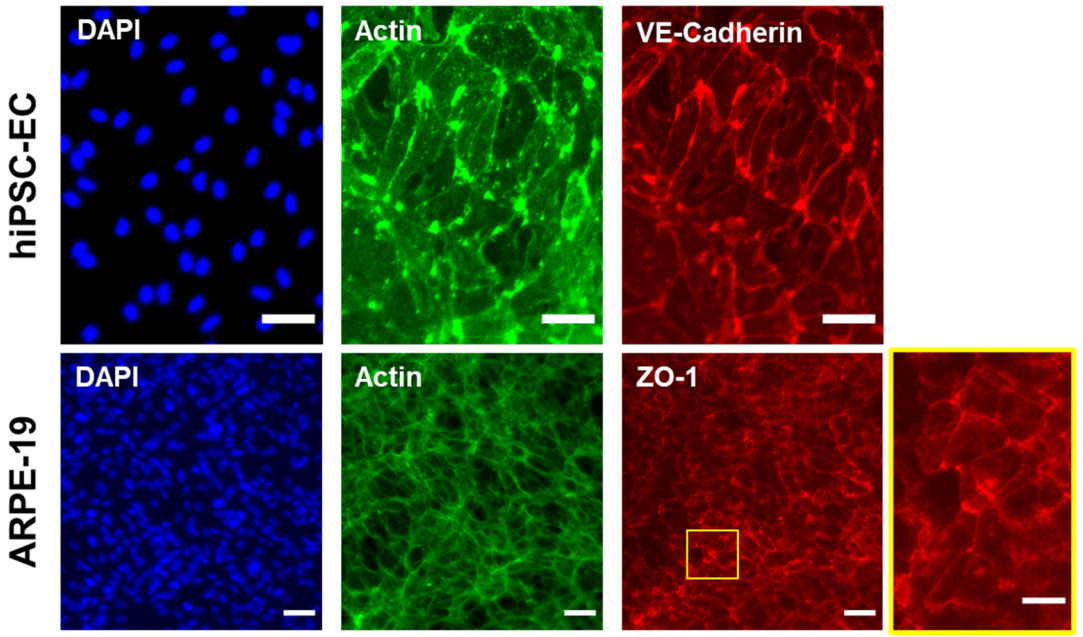


**Figure 2.** Collagen-based membranes are biocompatible and allow for adhesion and formation of monolayers of cells. Immunolabeling of cells on collagen-based membranes revealed a continuous distribution of each cell type indicated by DAPI (nuclei) and actin filament staining. These cells were positive for their respective cell−cell adhesion markers: VE-cadherin expression for hiPSC-EC and ZO-1 expression for ARPE-19, inset showing the highlighted area. Scale bars: 50 $\mu$m.

## RESULTS AND DISCUSSION

**Integration of Membrane to Devices.** Conventionally, integration of membranes to organ-on-a-chip devices, depending on the type of membranes, requires plasma activation of surfaces or application of PDMS mortar to adjacent surfaces between which membranes are incorporated.[33] Using a PDMS mortar in these devices requires the assembly of each device separately, which in turn increases the fabrication time. Here, in addition to mortar-based assembly of devices, we utilize injection molding as an alternative to conventional fabrication method. This eliminates the separate assembly of devices and significantly reduces the fabrication time (Figure 1C, Figure S5A). Integrated membranes are held between the channels by magnets from both ends. Resulting membranes do not contain any PDMS residues that is indicated by the absence of black PDMS on the membrane (Figure S5B).

**Production of Collagen I Based Bioresponsive Membranes.** In this study, we aim to mimic the native in vivo tissue interface provided by basal membranes. As the material of our membranes we chose collagen type I, because it is the most abundant protein in the human body. Moreover, one of the components of the basement membrane, basal lamina, anchors to the adjacent connective tissue using networks of type I collagen fibers in the reticular lamina.[21,34] In addition, type I collagen is found in specialized membranes such as Bruch's membrane, which facilitates nutrient/waste exchange between retinal pigment epithelium and choroidal capillaries in the retina and provides structural support for adjacent tissues.[35]

The fabrication process of the membrane relied on drying collagen I solutions on a nonadhesive PDMS surface. Fabrication did not require dedicated equipment and resulted in membranes with a thickness of ∼2 $\mu$m and a fibrillar structure (Figure 3A-I, Figure S4A). Membranes were prepared using a concentration of 3 mg/mL collagen I in the original solution. Lower concentrations resulted in membranes that were not sturdy enough to be handled.

In addition to single-layered membranes, we also fabricated double-layered membranes using membranes with collagen concentrations of 4 and 3 mg/mL. Cross-sectioning of these membranes were proven to be challenging as the fibrous structure does not separate well enough using the freeze fracture method; however, a multilayered structure can be deduced (Figure S4B).

These membranes also allow for cell culturing as evident in Figure 2. We obtained monolayers of cells lining the membrane surface indicated by the homogeneous distribution of nuclei and actin cytoskeleton stainings (Figure 2). Moreover, these cells grow to a healthy population as evident by their respective cell−cell adhesion markers (VE-cadherin for hiPSC-ECs, ZO-1 for ARPE-19). A healthy morphology can also be seen when these cells were seeded to glass coverslips, and express their respective markers (Figure S6). According to the manufacturer's information, collagen I from rat tail was isolated using acetic acid extraction without any further enzymatic treatment. As a result, in the final isolated proteins, telopeptide domains are intact. It has been reported by studies using porcine or bovine collagen that may illicit an immune response in planted microdevices or scaffolds in humans even though this is rare.[36] Moreover, to the best of our knowledge, a potential immune response to rat tail collagen was not reported by the manufacturer, and this does not cause any issues regarding a decrease in viability and attachment of cells.

**Enzymatic Degradation of Membranes.** During embryonic development, as well as in disease processes, multiple cell types traverse the barriers of the basal lamina.[37] These transmigrations are often associated with proteases, a class of enzymes responsible for remodeling the basement membranes. This has been supported by the observation of irreversible changes to the ECM during tissue-invasive events that are


https://dx.doi.org/10.1021/acsbiomaterials.0c00297
ACS Biomater. Sci. Eng. 2021, 7, 2998−3005

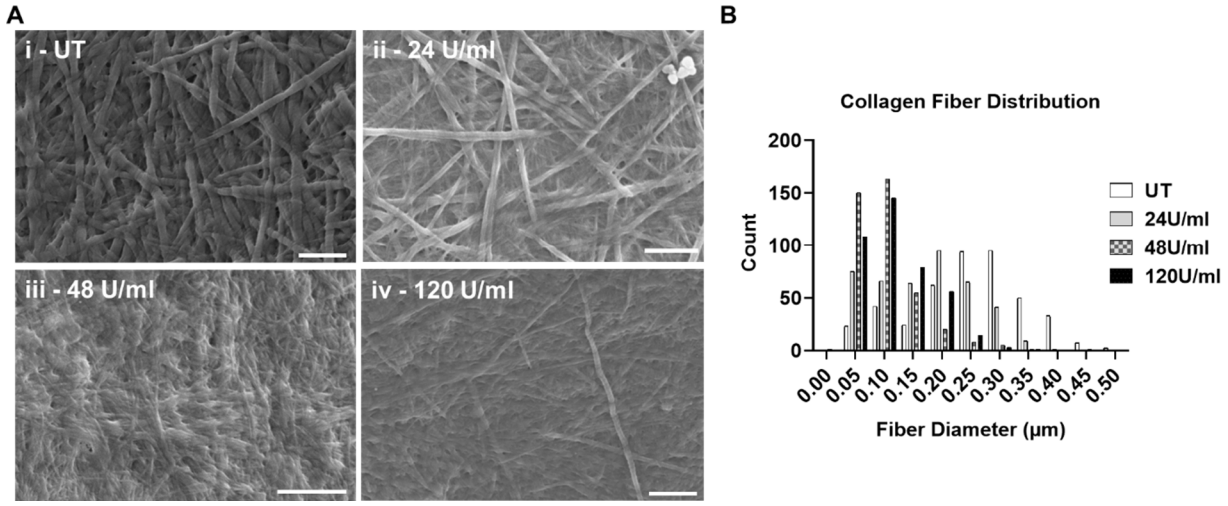


**Figure 3.** Characterization of collagen membranes following enzymatic treatment. (A) SEM images of membrane structure that are untreated or treated with various concentrations of collagenase-2 (24, 48, and 120 U/mL). Scale bars: 2 $\mu$m. (B) Distribution of fiber diameters of enzymatically treated membranes.

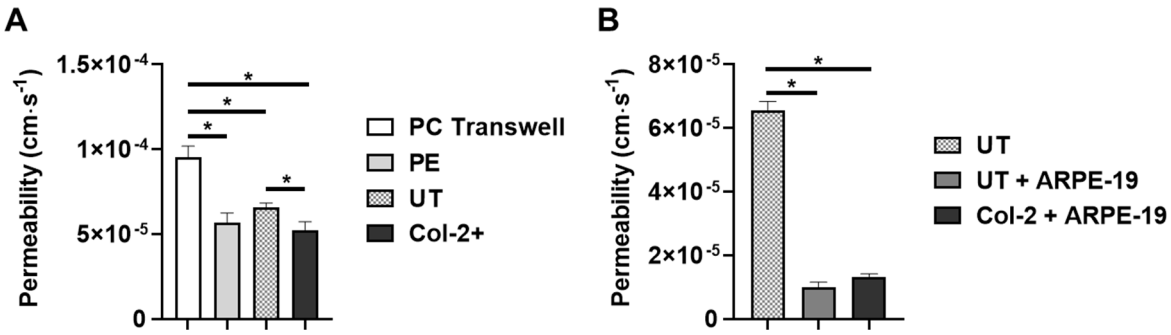


**Figure 4.** Collagen membranes were characterized in terms of permeability. (A) Permeability of various membranes were measured: Polycarbonate transwell membrane (PC Transwell), polyester (PE), collagen (UT), and enzymatically treated (Col-2+) membranes. Significant differences ($p < 0.05$, Student's $t$ test) are denoted by an asterisk. (B) Effect of cell seeding on collagen membranes by means of permeability. Nontreated collagen membranes (UT), nontreated membranes with ARPE-19 cells seeded (UT+ ARPE-19), and enzyme-treated membranes (Col-2+ ARPE-19) were measured. Significant differences according to one-way ANOVA and Posthoc Tukey's tests are indicated by asterisks.

associated with development and disease states.[37] For example, gaps in the basement membrane have been identified at sites of cancer invasion in vivo.[37−40] In addition, an increased expression of ECM degrading proteases has been observed in neoplastic epithelial cells.[41−43] Moreover, in retinal diseases such as the wet form of age-related macular degeneration, choroidal capillaries penetrate the Bruch's membrane and grow into the retina, leading to leakage of the contents, which leads to blindness. In patients, the expression of matrix remodeling enzymes are elevated.[44] These enzymes secreted by the surrounding vascular endothelium and macrophages degrade the extracellular matrix, which allows infiltration of Bruch's membrane by the adjacent capillaries.[45,46] Given the importance of basement membrane remodeling in development and disease, we set out to study the enzymatic remodeling of our vitrified collagen membranes.

We treated the membranes with collagenase-2 to affect their structure and properties. We selected this enzyme because it has been used in tissue dissociation and is extensively characterized.[47] Because of its potency in tissue dissociation, we exposed the membranes to relatively low concentrations (24, 48, or 120 U/mL) for a short duration of 5 min. Membranes that were treated longer or with higher enzyme concentrations became unstable and easily fractured during permeability measurements (Figure S2).

SEM imaging of membranes treated with collagenase showed striking differences in morphology between treatment conditions. Single collagen I fibers can easily be distinguished from one another in the untreated membranes (Figure 3A-i). However, upon treatment with increasing concentrations of collagenase (Figure 3A-ii−iv) this clarity is lost. Moreover, there is a dose-dependent trend in terms of fiber diameters when compared to untreated membranes. In treated membranes, the majority of fibers have a diameter of 50 nm, in contrast to untreated membranes in which diameters exhibited a broad distribution from 50 to 400 nm. (Figure 3B). This observation is in line with existing information about the fiber size as it ranges between 50 and 200 nm in diameter.[48] The morphological changes upon treatment with collagenase are in line with its mechanism of action, which depends on cleavage of the triple helix of collagen at multiple sites. As a result, fiber thinning occurs.[49,50]

Considering the importance of diffusion of solutes across a barrier in modeling barrier tissues that many organ-on-a-chip platforms tackle, we characterized the membranes in terms of permeability by measuring the diffusion of fluorescein (Figure 4). First, we measured the permeability on membranes in


https://dx.doi.org/10.1021/acsbiomaterials.0c00297
ACS Biomater. Sci. Eng. 2021, 7, 2998−3005

which cells were not cultured. On the basis of these measurements, collagen membranes showed a comparable permeability to polyester membranes, which we incorporated in our devices (Figure 4A). Apparent permeability values of membranes in our devices were significantly lower overall than the polycarbonate membranes in Transwell inserts (Figure 4A). This difference might be due to minor advective transport due to a pressure gradient over the membranes in the devices. Here, it is worth noting that the polycarbonate and polyester membranes have the same pore density and pore size. In addition, upon treatment with collagenase, membrane permeability was significantly lowered (Figure 4A). This might be due to the partial degradation of collagen fibers, with the degraded material forming a gelatin hydrogel. This would decrease the open porous structure and thereby lower the amount of fully open paths between fibers through which fluorescein can diffuse. In addition to this decreased porosity, one of the collagenase isoforms present in our enzyme, clostripain, can act as a transpeptidase, which may cross-link the fiber fragments resulting in the formation of a gelatin film.[49] Higher collagenase concentrations or treatment times caused membranes to burst or puncture, thus they were not taken into consideration for permeability measurements (Figure S2).

As a next step, we measured the permeability of membranes that were incorporated in the devices and on which ARPE-19 cells were cultured. We performed the permeability measurements after 3 days of culturing to ensure a healthy monolayer on the membranes (Figure S3). Here, according to our measurements, ARPE-19 growing on membranes significantly lowered the permeability (Figure 4B), indicating the formation of a tight monolayer of these epithelial cells. Upon treatment of these cultures with collagenase, no significant effect on the permeability was observed, presumably because the ARPE-19 monolayer shields the membrane from the soluble enzyme (Figure 4B).

This result also highlights the fact that cells are the main diffusion barrier to small molecules just as is the case in healthy in vivo situation, and that the VC membrane does not significantly interfere in the diffusion process.

## CONCLUSIONS

As current cellular and animal models fail at fully recapitulating the in vivo microenvironment of human organs and tissues, organ-on-a-chip systems have great potential in investigating disease pathology and organ-level physiology. These systems incorporate various cell types from the human body as well as clinically relevant readouts. To that end, we aimed to eliminate the usage of synthetic membranes as they are not an actual part of the in vivo ECM. Here we reported a collagen I based membrane that can be incorporated in organs-on-chips and which we characterized in terms of cell adhesion, ultrastructure, and permeability. We demonstrated that these membranes can be treated with proteases and changes in fiber thickness and permeability can be evaluated. Our results provide actual quantitative permeability values that can be compared with future studies.

As a next step, different ECM proteins like collagen IV and laminin can be integrated into our membrane fabrication to generate an even more representative model of the basement membrane.

## ASSOCIATED CONTENT

### Supporting Information

The Supporting Information is available free of charge at https://pubs.acs.org/doi/10.1021/acsbiomaterials.0c00297.

Schematic overview of the permeability measurements by means of fluorescein diffusion; rupture of membranes due to high concentrations of enzymatic treatment; ARPE-19 cells cultured on membranes; SEM images of single and multilayered membranes; schematic overview of injection molding design and membrane from resulting assembled devices; ARPE-19 cells grown on collagen-I coated coverslips (PDF)

## AUTHOR INFORMATION


### Corresponding Author

**Andries D. van der Meer** − *Applied Stem Cell Technologies, Technical Medical Centre, University of Twente, Enschede 7500 AE, The Netherlands*; Email: andries.vandermeer@utwente.nl

### Authors

**Yusuf B. Arık** − *Applied Stem Cell Technologies, Technical Medical Centre and BIOS Lab on a Chip group, Technical Medical Centre, MESA+ Institute for Nanotechnology, University of Twente, Enschede 7500 AE, The Netherlands*; orcid.org/0000-0001-9528-0145

**Aisen de sa Vivas** − *Applied Stem Cell Technologies, Technical Medical Centre and BIOS Lab on a Chip group, Technical Medical Centre, MESA+ Institute for Nanotechnology, University of Twente, Enschede 7500 AE, The Netherlands*

**Daphne Laarveld** − *Applied Stem Cell Technologies, Technical Medical Centre, University of Twente, Enschede 7500 AE, The Netherlands*

**Neri van Laar** − *Applied Stem Cell Technologies, Technical Medical Centre, University of Twente, Enschede 7500 AE, The Netherlands*

**Jesse Gemser** − *Applied Stem Cell Technologies, Technical Medical Centre, University of Twente, Enschede 7500 AE, The Netherlands*

**Thomas Visscher** − *Applied Stem Cell Technologies, Technical Medical Centre, University of Twente, Enschede 7500 AE, The Netherlands*

**Albert van den Berg** − *BIOS Lab on a Chip group, Technical Medical Centre, MESA+ Institute for Nanotechnology, University of Twente, Enschede 7500 AE, The Netherlands*

**Robert Passier** − *Applied Stem Cell Technologies, Technical Medical Centre, University of Twente, Enschede 7500 AE, The Netherlands; Department of Anatomy and Embryology, Leiden University Medical Center, Leiden 2300 RC, The Netherlands*

Complete contact information is available at: https://pubs.acs.org/10.1021/acsbiomaterials.0c00297


### Author Contributions

Y.B.A., A.D.S.V., and A.D.M. designed the experiments and critically analyzed data. Y.B.A. performed the chip design. D.L., N.V.L., J.G., and T.V. fabricated collagen membranes, maintained cell cultures on membranes, and performed immunofluorescent stainings. D.L. and T.V. performed the permeability measurements on nontreated and enzymatically treated membranes. R.P. and A.B. critically advised on data and reviewed the manuscript.



https://dx.doi.org/10.1021/acsbiomaterials.0c00297
ACS Biomater. Sci. Eng. 2021, 7, 2998−3005

### Author Contributions

†Y.B.A. and A.d.s.V. contributed equally.

### Funding

The authors acknowledge the funding received from Stichting Toegepast Wetenschappelijk Instituut voor Neuromodulatie (TWIN) under the project 'Inflammation and Edema in an Organ-on-a-Chip Model of Wet Age-Related Macular Degeneration', from the Dutch Science Foundation (NWO) under the "VESCEL" Program (Grant 669768) of Prof. Albert van den Berg.

### Notes

The authors declare no competing financial interest.

## REFERENCES

(1) Frantz, C.; Stewart, K. M.; Weaver, V. M. The extracellular matrix at a glance. *J. Cell Sci.* **2010**, *123* (24), 4195−4200.
(2) Rosso, F.; Giordano, A.; Barbarisi, M.; Barbarisi, A. From cell−ECM interactions to tissue engineering. *J. Cell. Physiol.* **2004**, *199* (2), 174−180.
(3) Keely, P. J.; Fong, A. M.; Zutter, M. M.; Santoro, S. A. Alteration of collagen-dependent adhesion, motility, and morphogenesis by the expression of antisense alpha 2 integrin mRNA in mammary cells. *J. Cell Sci.* **1995**, *108* (2), 595−607.
(4) Järveläinen, H.; Sainio, A.; Koulu, M.; Wight, T. N.; Penttinen, R. Extracellular matrix molecules: potential targets in pharmacotherapy. *Pharmacol. Rev.* **2009**, *61* (2), 198−223.
(5) Huh, D.; Matthews, B. D.; Mammoto, A.; Montoya-Zavala, M.; Hsin, H. Y.; Ingber, D. E. Reconstituting organ-level lung functions on a chip. *Science* **2010**, *328* (5986), 1662−1668.
(6) van der Meer, A. D.; van den Berg, A. Organs-on-chips: breaking the in vitro impasse. *Integr. Biol.* **2012**, *4* (5), 461−470.
(7) Du, G.; Fang, Q.; den Toonder, J. M. Microfluidics for cell-based high throughput screening platforms—A review. *Anal. Chim. Acta* **2016**, *903*, 36−50.
(8) Bhatia, S. N.; Ingber, D. E. Microfluidic organs-on-chips. *Nat. Biotechnol.* **2014**, *32* (8), 760.
(9) Loskill, P.; Sezhian, T.; Tharp, K. M.; Lee-Montiel, F. T.; Jeeawoody, S.; Reese, W. M.; Zushin, P.-J. H.; Stahl, A.; Healy, K. E. WAT-on-a-chip: a physiologically relevant microfluidic system incorporating white adipose tissue. *Lab Chip* **2017**, *17* (9), 1645−1654.
(10) Hutson, M. S.; Alexander, P. G.; Allwardt, V.; Aronoff, D. M.; Bruner-Tran, K. L.; Cliffel, D. E.; Davidson, J. M.; Gough, A.; Markov, D. A.; McCawley, L. J.; et al. Organs-on-chips as bridges for predictive toxicology. *Appl. In Vitro Toxicol.* **2016**, *2* (2), 97−102.
(11) Bergers, L.; Waaijman, T.; De Gruijl, T.; Van De Stolpe, A.; Dekker, R.; Gibbs, S. Skin-on-chip: Integrating skin-tissue and microsystems engineering. *Tissue Eng., Part A* **2015**, *21*, S337−S338.
(12) Marx, U.; Walles, H.; Hoffmann, S.; Lindner, G.; Horland, R.; Sonntag, F.; Klotzbach, U.; Sakharov, D.; Tonevitsky, A.; Lauster, R. 'Human-on-a-chip'developments: a translational cutting-edge alternative to systemic safety assessment and efficiency evaluation of substances in laboratory animals and man? *ATLA, Altern. Lab. Anim.* **2012**, *40* (5), 235.
(13) Tibbe, M. P.; van der Meer, A. D.; van den Berg, A.; Stamatialis, D.; Segerink, L. Membranes for Organs-On-Chips. In *Biomedical Membranes and (Bio)Artificial Organs*; World Scientific Series in Membrane Science and Technology: Biological and Biomimetic Applications, Energy and the Environment; World Scientific: Singapore, 2018; Vol. 2, Chapter 11, pp 295−321.
(14) Cooke, M.; Phillips, S.; Shah, D.; Athey, D.; Lakey, J.; Przyborski, S. Enhanced cell attachment using a novel cell culture surface presenting functional domains from extracellular matrix proteins. *Cytotechnology* **2008**, *56* (2), 71−79.
(15) Albuschies, J.; Vogel, V. The role of filopodia in the recognition of nanotopographies. *Sci. Rep.* **2013**, *3*, 1658.
(16) Neeves, K. B.; Diamond, S. L. A membrane-based microfluidic device for controlling the flux of platelet agonists into flowing blood. *Lab Chip* **2008**, *8* (5), 701−709.
(17) Iliescu, C.; Taylor, H.; Avram, M.; Miao, J.; Franssila, S. A practical guide for the fabrication of microfluidic devices using glass and silicon. *Biomicrofluidics* **2012**, *6* (1), 016505.
(18) Das, P.; Van Der Meer, A. D.; Vivas, A.; Arik, Y. B.; Remigy, J.-C.; Lahitte, J.-F.; Lammertink, R. G.; Bacchin, P. Tunable microstructured membranes in organs-on-chips to monitor transendothelial hydraulic resistance. *Tissue Eng., Part A* **2019**, *25* (23−24), 1635−1645.
(19) Liu, Y.; Yang, D.; Yu, T.; Jiang, X. Incorporation of electrospun nanofibrous PVDF membranes into a microfluidic chip assembled by PDMS and scotch tape for immunoassays. *Electrophoresis* **2009**, *30* (18), 3269−3275.
(20) Miura, S.; Sato, K.; Kato-Negishi, M.; Teshima, T.; Takeuchi, S. Fluid shear triggers microvilli formation via mechanosensitive activation of TRPV6. *Nat. Commun.* **2015**, *6* (1), 1−11.
(21) Mondrinos, M. J.; Yi, Y.-S.; Wu, N.-K.; Ding, X.; Huh, D. Native extracellular matrix-derived semipermeable, optically transparent, and inexpensive membrane inserts for microfluidic cell culture. *Lab Chip* **2017**, *17* (18), 3146−3158.
(22) Takezawa, T.; Takeuchi, T.; Nitani, A.; Takayama, Y.; Kinooka, M.; Taya, M.; Enosawa, S. Collagen vitrigel membrane useful for paracrine assays in vitro and drug delivery systems in vivo. *J. Biotechnol.* **2007**, *131* (1), 76−83.
(23) Puleo, C. M.; McIntosh Ambrose, W.; Takezawa, T.; Elisseeff, J.; Wang, T.-H. Integration and application of vitrified collagen in multilayered microfluidic devices for corneal microtissue culture. *Lab Chip* **2009**, *9* (22), 3221−3227.
(24) Choi, Y.; Hyun, E.; Seo, J.; Blundell, C.; Kim, H. C.; Lee, E.; Lee, S. H.; Moon, A.; Moon, W. K.; Huh, D. A microengineered pathophysiological model of early-stage breast cancer. *Lab Chip* **2015**, *15* (16), 3350−3357.
(25) Takezawa, T.; Nishikawa, K.; Wang, P.-C. Development of a human corneal epithelium model utilizing a collagen vitrigel membrane and the changes of its barrier function induced by exposing eye irritant chemicals. *Toxicol. In Vitro* **2011**, *25* (6), 1237−1241.
(26) Majumdar, S.; Guo, Q.; Garza-Madrid, M.; Calderon-Colon, X.; Duan, D.; Carbajal, P.; Schein, O.; Trexler, M.; Elisseeff, J. Influence of collagen source on fibrillar architecture and properties of vitrified collagen membranes. *J. Biomed. Mater. Res., Part B* **2016**, *104* (2), 300−307.
(27) Iwadate, H.; Yamada, M.; Kimura, N.; Hashimoto, R.; Yajima, Y.; Utoh, R.; Seki, M. PDMS microstencil plate-supported fabrication of ultra-thin, condensed ECM membranes for separated cell coculture on both surfaces. *Sens. Actuators, B* **2019**, *287*, 486−495.
(28) Takezawa, T.; Ozaki, K.; Nitani, A.; Takabayashi, C.; Shimo-Oka, T. Collagen vitrigel: a novel scaffold that can facilitate a three-dimensional culture for reconstructing organoids. *Cell transplantation* **2004**, *13* (4), 463−474.
(29) Lo, J. H.; Bassett, E. K.; Penson, E. J.; Hoganson, D. M.; Vacanti, J. P. Gas transfer in cellularized collagen-membrane gas exchange devices. *Tissue Eng., Part A* **2015**, *21* (15−16), 2147−2155.
(30) Griep, L. M.; Wolbers, F.; de Wagenaar, B.; ter Braak, P. M.; Weksler, B.; Romero, I. A.; Couraud, P.; Vermes, I.; van der Meer, A. D.; van den Berg, A. BBB on chip: microfluidic platform to mechanically and biochemically modulate blood-brain barrier function. *Biomed. Microdevices* **2013**, *15* (1), 145−150.
(31) van der Helm, M. W.; Odijk, M.; Frimat, J.-P.; van der Meer, A. D.; Eijkel, J. C.; van den Berg, A.; Segerink, L. I. Fabrication and validation of an organ-on-chip system with integrated electrodes to directly quantify transendothelial electrical resistance. *J. Visualized Exp.* **2017**, No. 127, e56334.
(32) Orlova, V. V.; Van Den Hil, F. E.; Petrus-Reurer, S.; Drabsch, Y.; Ten Dijke, P.; Mummery, C. L. Generation, expansion and functional analysis of endothelial cells and pericytes derived from human pluripotent stem cells. *Nat. Protoc.* **2014**, *9* (6), 1514−1531.


https://dx.doi.org/10.1021/acsbiomaterials.0c00297
ACS Biomater. Sci. Eng. 2021, 7, 2998−3005

(33) Chueh, B.-h.; Huh, D.; Kyrtsos, C. R.; Houssin, T.; Futai, N.; Takayama, S. Leakage-free bonding of porous membranes into layered microfluidic array systems. *Anal. Chem.* **2007**, *79* (9), 3504−3508.
(34) Yurchenco, P. D. Basement membranes: cell scaffoldings and signaling platforms. *Cold Spring Harbor Perspect. Biol.* **2011**, *3* (2), a004911.
(35) Curcio, C. A.; Johnson, M. Structure, function, and pathology of Bruch's membrane. *Retina* **2013**, *1* (Part 2), 465−481.
(36) Lynn, A.; Yannas, I.; Bonfield, W. Antigenicity and immunogenicity of collagen. *J. Biomed. Mater. Res.* **2004**, *71* (2), 343−354.
(37) Rowe, R. G.; Weiss, S. J. Breaching the basement membrane: who, when and how? *Trends Cell Biol.* **2008**, *18* (11), 560−574.
(38) Spaderna, S.; Schmalhofer, O.; Hlubek, F.; Berx, G.; Eger, A.; Merkel, S.; Jung, A.; Kirchner, T.; Brabletz, T. A transient, EMT-linked loss of basement membranes indicates metastasis and poor survival in colorectal cancer. *Gastroenterology* **2006**, *131* (3), 830−840.
(39) Frei, J. The fine structure of the basement membrane in epidermal tumors. *J. Cell Biol.* **1962**, *15* (2), 335−342.
(40) Wheatley, D. An electron microscopic study of the invasion of ascites tumor cells into the abdominal wall. *Cancer Res.* **1965**, *25* (4 Part 1), 490−497.
(41) Sherwood, D. R. Cell invasion through basement membranes: an anchor of understanding. *Trends Cell Biol.* **2006**, *16* (5), 250−256.
(42) Christofori, G. New signals from the invasive front. *Nature* **2006**, *441* (7092), 444−450.
(43) Page-McCaw, A.; Ewald, A. J.; Werb, Z. Matrix metalloproteinases and the regulation of tissue remodelling. *Nat. Rev. Mol. Cell Biol.* **2007**, *8* (3), 221−233.
(44) Leu, S. T.; Batni, S.; Radeke, M. J.; Johnson, L. V.; Anderson, D. H.; Clegg, D. O. Drusen are cold spots for proteolysis: expression of matrix metalloproteinases and their tissue inhibitor proteins in age-related macular degeneration. *Exp. Eye Res.* **2002**, *74* (1), 141−154.
(45) Bhutto, I.; Lutty, G. Understanding age-related macular degeneration (AMD): relationships between the photoreceptor/retinal pigment epithelium/Bruch's membrane/choriocapillaris complex. *Mol. Aspects Med.* **2012**, *33* (4), 295−317.
(46) Grossniklaus, H. E.; Green, W. R. Choroidal neovascularization. *Am. J. Ophthalmol.* **2004**, *137* (3), 496−503.
(47) Warwick, D.; Arandes-Renú, J. M.; Pajardi, G.; Witthaut, J.; Hurst, L. C. Collagenase Clostridium histolyticum: emerging practice patterns and treatment advances. *Journal of plastic surgery and hand surgery* **2016**, *50* (5), 251−261.
(48) Lodish, H.; Berk, A.; Zipursky, S. L.; Matsudaira, P.; Baltimore, D.; Darnell, J., Collagen: the fibrous proteins of the matrix. In *Molecular Cell Biology*, 4th ed.; W. H. Freeman: New York, 2000; Vol. 4.
(49) Van Wart, H. E., Clostridium collagenases. In *Handbook of Proteolytic Enzymes*; Elsevier, 2004; pp 416−419.
(50) Wang, X.; Huang, Y.; Jastaneiah, S.; Majumdar, S.; Kang, J. U.; Yiu, S. C.; Stark, W.; Elisseeff, J. H. Protective effects of soluble collagen during ultraviolet-A crosslinking on enzyme-mediated corneal ectatic models. *PLoS One* **2015**, *10* (9), e0136999.


https://dx.doi.org/10.1021/acsbiomaterials.0c00297
*ACS Biomater. Sci. Eng.* 2021, 7, 2998−3005